Identification of SLC25A46 interaction interfaces with mitochondrial membrane fusogens Mfn2 and Opa1

Sivakumar Boopathy[1,2], Camila Makhlouta Lugo[1*], Bridget E. Luce[1], Julie McDonald[1#], Pusparanee Hakim[1], Jackeline Ponce[3], Beatrix M. Ueberheide[3,4], Luke H. Chao[1,2,5]

[1]Department of Molecular Biology, Massachusetts General Hospital, Boston MA 02114, USA

[2]Department of Genetics, Harvard Medical School, Boston MA 02115, USA

3 Proteomics Resource Center, Division of Advanced Research Technologies, New York University Langone Health Center, New York NY 10016, USA

[4]Department of Biochemistry and Molecular Pharmacology, New York University Langone Health Center, New York NY 10016, USA

[5]Corresponding author

*Present address: Program in Neurobiology, University of Chicago, Chicago IL 60637, USA

[#]Present address: Department of Biology, Massachusetts Institute of Technology, Cambridge MA 02139, USA

Running Title

SLC25A46 interaction interfaces with Mfn2 and Opa1

Keywords

1. Mitochondria
2. Membrane fusion
3. GTPase
4. Structural model
5. Protein cross-linking
6. Mass spectrometry
7. Protein-protein interaction
8. Mitochondrial solute carrier

Abstract

Mitochondrial fusion requires the sequential merger of four bilayers to two. The outer-membrane solute carrier protein SLC25A46 interacts with both the outer and inner-membrane dynamin family GTPases Mfn1/2 and Opa1. While SLC25A46 levels are known affect mitochondrial morphology, how SLC25A46 interacts with Mfn1/2 and Opa1 to regulate membrane fusion is not understood. In this study, we use crosslinking mass-spectrometry and AlphaFold 2 modeling to identify interfaces mediating a SLC25A46-Opa1-Mfn1/2 complex. We reveal that the bundle signaling element of Opa1 interacts with SLC25A46, and the helical repeat 1 region of Mfn2 interacts with the SLC25A46 N-terminus. We validate these newly identified interaction interfaces and show that they play a role in mitochondrial network maintenance.

Introduction

Mitochondrial fission and fusion are membrane remodeling processes required for maintenance of a healthy mitochondrial reticulum (1, 2), which regulates the number, and distribution of mitochondrial DNA and respiratory chain proteins (1-5). A distinct feature of mitochondrial fusion is the sequential fusion of two pairs of bilayers. Key questions regarding the spatiotemporal control of these events remain. Specifically, how are the activities of the outer and inner membrane fusion GTPases, Mfn1/2 and Opa1 respectively, coordinated and regulated?

SLC25A46 interacts with both fusion GTPases and has emerged as an inter-membrane bridging protein which plays roles in regulating mitochondrial membrane dynamics (6-9). Mutations in SLC25A46 result in optic atrophy spectrum disorder, Leigh syndrome, and pontocerebellar hypoplasia (10-24). SLC25A46 is a member of the solute carrier family 25 of mitochondrial transporters, which transport substrates such as nucleotides, vitamins, amino acids, fatty acids across the inner mitochondrial membrane (IMM) (25). SLC25A46 resides in the outer mitochondrial membrane (OMM), lacks the signature sequence motifs of the SLC25 family (25), does not have an identified substrate and contains a distinct N-terminal extension.

In SLC25A46 knockout and knockdown models of human neurological disease, mitochondria are often enlarged and aggregated in nervous tissues, exhibiting detached, vesiculated cristae (21, 24, 26-29). Respiratory chain complex activity is impaired in these models (26, 27), and ATP levels are reduced (27, 28). In human cell lines, knockdown of SLC25A46 induces a tubular mitochondrial network whereas overexpression results in mitochondrial fragmentation (6, 9, 24), suggesting a role in downregulating fusion. The phenotypes of SLC25A46 knockout varied depending on the cell lines tested, displaying mitochondrial fragmentation in human fibroblasts and HeLa cells (8), and hyper-filamentous network in other cell lines (30, 31). Knockout of the yeast orthologoue Ugo1 (~22% sequence identity) also induced fragmentation (32-34). These observations argue for a role of SLC25A46 in regulating mitochondrial fusion where SLC25A46 levels at the OMM are critical. In fibroblasts and iPSC-derived cerebral neurons, SLC25A46 is focally present at tips and branches of mitochondrial tubules and at sites of fusion and fission (8). Interestingly the SLC25A46 puncta were

proximal to Opa1 in human fibroblasts (8), suggesting spatially-defined interactions with SLC25A46 play a role in fusion regulation.

Understanding the molecular details of the SLC25A46-Mfn2-Opa1 interactions can provide constraints on how SLC25A46 organizes sites for mitochondrial membrane remodeling and inform mechanisms for coordinated OMM/IMM fusion. In yeast, Ugo1 physically interacts with Fzo1 and Mgm1, the orthologous fusion GTPases (34-37). Previous studies indicate Opa1 and Mfn2 interacts with SLC25A46 (6-9), however the specific interface mediating these interactions was undefined. In this study, we used crosslinking-mass spectrometry and AlphaFold 2 modeling to identify the protein-protein interaction surfaces of SLC25A46-Opa1 and SLC25A46-Mfn2. We validated this newly identified SLC25A46-Opa1 interface by mutagenesis, and demonstrate a role for this interface in mitochondrial network maintenance.

Results

SLC25A46 interacts with Opa1 via its bundle signaling element.

Previous studies used crosslinking, immunoprecipitation and mass spectrometry to identify an interaction network of Opa1, Mfn1/2 and SLC25A46 (6-9). We over-expressed human SLC25A46 with Opa1 in *Pichia pastoris* under the control of a strong promoter (alcohol oxidase) (**Figure 1A**), and found that detergent (GDN)-solubilized SLC25A46 in *P. pastoris* lysate interacts with column-immobilized Opa1 from lysate in the absence of crosslinkers (**Figure 1B**). Likewise, column-immobilized SLC25A46 was also found to interact with Opa1 (**Supporting Figure 1A**).

To identify the specific interface responsible for the SLC25A46-Opa1 interaction, we crosslinked the purified complex for analysis by mass spectrometry. Using bis(sulfosuccinimidyl)suberate (BS3) we identified a crosslink between K241 of SLC25A46 and K568 of Opa1 bundle signaling element (BSE) helix 2. Intralinks consistent with folded Opa1 secondary structure elements were identified (**Supporting Figure 1B**). A second crosslinker Bis-N-succinimidyl-(pentaethylene glycol) (BS(PEG)5) with a larger spacer length also crosslinked K241(SLC25A46)-K568(Opa1), and identified a second crosslink between K256 of SLC25A46 and the K960 of Opa1 BSE helix 3 (**Figure 1C**). We modeled this interaction using Alphafold 2 (38, 39), which

consistently revealed a high-confidence and robust interface mediated by the Opa1 BSE, with a topology consistent with the proteins' sub-organellar localization (6, 21, 24, 40, 41) (**Figure 1D, Supporting Figure 1C**).

Validation of SLC25A46:Opa1-BSE interaction

Examination of the SLC25A46-Opa1 interface in the AlphaFold 2 model revealed two salt bridges comprising residues R257 (SLC25A46) and E561 (Opa1); R347 (SLC25A46) and D565 (Opa1). Adjacent to the salt bridges, a cluster of hydrophobic residues, I229, I230, I349, Y357, V359, L360 in SLC25A46 and A569, F572 and T576 in Opa1 BSE helix 2 appear to further stabilize the interaction (**Supporting Figure 2A**). We tested this newly identified SLC25A46-Opa1 interface by mutating the salt bridges and hydrophobic site residues in SLC25A46, and evaluating if the interaction with Opa1 was maintained (**Figure 2A**). While recombinantly expressed and purified WT SLC25A46 bound column-immobilized Opa1 (consistent with observations in lysates), both the I349D mutation and the R257A/R347A double mutation diminished the interaction (**Figure 2B and Supporting Figure 2B**).

The BSE is essential for transducing GTP-hydrolysis stimulated activities of dynamin related protein (42, 43). In dynamin, the BSE frequently moves closer to the GTPase upon GTP hydrolysis (44-46). To determine if the nucleotide-state of Opa1 affects its interaction with SLC25A46, we incubated the lysates with GTPγS, GMPPCP and GDP prior to affinity capture on StrepTactin resin. We found that the presence of nucleotide or nucleotide analogues did not affect co-elution, indicating nucleotide-coupled BSE rearrangement does not affect Opa1-SLC25A46 interaction (**Supporting Figure 2C**).

We also generated a minimal construct consisting of the GTPase domain and the BSE alone (Opa1(MGD)), to test that the "paddle" and stalk self-assembly regions are dispensable for the Opa1-SLC25A46 interaction (**Figure 3A**). SLC25A46 bound Opa1(MGD) as shown by the co-elution of the two proteins, indicating an Opa1(MGD) construct is sufficient for binding (**Figure 3B**). We found the same two crosslinks observed for Opa1-SLC25A46 between Opa1(MGD) and SLC25A46. In addition, we

observed a third crosslink between K387 of SLC25A46 and K568 of Opa1 (**Figure 3C and 3D**).

The cytosolic unstructured domain of SLC25A46 interacts with the HR1 of Mfn2.

We next investigated if SLC25A46 also interacts with the outer membrane fusion protein Mfn2. We co-expressed the two proteins in *P. pastoris* (**Supporting Figure 3A**) and subjected the GDN-solubilized lysates to column-binding experiments. SLC25A46 co-elutes upon elution of column-immobilized Mfn2 (**Supporting Figure 3B**), and Mfn2 co-elutes with resin bound SLC25A46 (**Supporting Figure 3C**). To test the SLC25A46-Mfn2 interaction was nucleotide-state dependent, we treated lysates with GTPγS, GMPPCP or GDP during detergent extraction. The presence of these nucleotides did not enhance or diminish interaction of Mfn2 with SLC25A46 (**Supporting Figure 3H**).

To obtain insights into the SLC25A46-Mfn2 interaction, we performed crosslinking and mass-spectrometry of the purified complex. Two crosslinks were identified – between K60 residue of SLC25A46 and residues K416 and K420 of Mfn2 (**Supporting Figure 3D**). K60 of SLC25A46 is part of the first ~83 residues that are predicted to be disordered in the cytosol (**Supporting Figure 3F**). Residues K416 and K420 are part of the cytosol facing heptad repeat 1 (HR1) of Mfn2 (**Supporting Figure 3F**). The AlphaFold 2 predicted interface was low confidence for SLC25A46-Mfn2 complex, particularly for the N-terminal region of SLC25A46.

Since crosslinks were observed at K60 in SLC25A46, we tested the role of these N-terminal residues in binding Mfn2. We deleted the first 83 amino acids of SLC25A46 termed (Δ2-83)SLC25A46, and co-expressed this protein with Mfn2 in *P. pastoris*. Interestingly, (Δ2-83)SLC25A46 still co-eluted with Mfn2 in the affinity capture experiments (**Supporting Figure 3G**).

Disease-causing SLC25A46 mutants do not affect interaction with Opa1 or Mfn2.

A cluster of SLC25A46 disease mutations face the IMS (**Figure 4A**). While many mutations were reported to destabilize the protein, certain disease-causing mutations (T142I and R340C) cause a hyper-fused mitochondrial phenotype (6, 8, 9, 15, 24). We co-expressed these SLC25A46 mutants with Opa1, and found these disease mutants

still bound Opa1 (**Figure 4B**). We note that in these experiments we were unable to achieve similar expression levels of the various proteins. We also saw no effect of patient-derived mutations on the Mfn2-SLC25A46 interaction (**Supporting Figure 3G**).

Mutations disrupting SLC25A46-Opa1 interaction alter mitochondrial morphology.

Previous studies showed that the pathogenic mutants of SLC25A46 that are unstable and express poorly in cells (6, 8, 9, 15, 21) induce a hyper-filamentous phenotype similar to that observed with siRNA/shRNA knockdown of SLC25A46 (6, 9, 24). To revisit mitochondrial phenotypes upon SLC25A46 loss, we imaged mitochondrial networks in the human colorectal carcinoma cell line HCT116. Loss of SLC25A46 did not affect mitochondrial morphology in HCT116 cells, but upon serum starvation, a fragmented mitochondrial network was observed. Reintroduction of WT SLC25A46 rescued this phenotype (**Figure 5, Supporting Video 1**). This phenotype is consistent with previous observations in human fibroblasts and HeLa cells (8). We found that expression of R340C or R257Q SLC25A46 mutants induced interconnected mitochondria, also in agreement with previous studies (8, 24) (**Figure 5B, Supporting Video 1**). The mitochondrial morphology in G249D-expressing cells was similar to WT (**Figure 5, Supporting Video 1**). Expression levels of R340C and G249D mutants never reached WT-like levels (**Figure 5A**), likely due to protein instability (6, 8, 9, 15, 21).

We next tested the effects of the newly identified Opa1-SLC25A46 interactions on mitochondrial morphology. Expression of I349D SLC25A46 (disrupts a hydrophobic interface between the Opa1 BSE) produced shorter mitochondrial tubules compared to WT, whereas R257A/R347A mutant (disrupt SLC25A46-Opa1 salt bridge interactions) resulted in more fragmented mitochondria (**Figure 5B, Supporting Video 1**). These results suggest that the identified SLC24A45-Opa1 interaction interface is important for maintaining a tubular mitochondrial morphology. Expression of the (Δ2-83)SLC25A46 resulted in an increase in short mitochondrial tubules (**Figure 5B, Supporting Video 1**). In these experiments, we did not observe changes in levels of Mfn2 or Opa1 due to SLC25A46 knockout or expression of varying levels of mutant SLC25A46 (**Figure 5A**).

We could not evaluate the expression level of (Δ2-83)SLC25A46 due to the inability of commercial antibodies to detect this mutant (**Figure 5A**).

Discussion

Mitochondria undergo morphological changes tightly coupled to cellular physiology (4). While the identity of the GTPases responsible for sequential mitochondrial fusion have long been identified (47), and mechanisms for individual fusion steps have been described (48-51), questions remain regarding how outer and inner-membrane activities are coordinated and regulated. Emerging evidence points to SLC25A46 as a regulator of fusion activity, with protein levels influencing the fusion-fission balance (6, 8, 24). Consistent with this role, SLC25A46 is observed to localize to the fusion sites (8).

In this study, we investigate the physical interaction between SLC25A46 and the membrane fusogens Opa1 and Mfn1/2. Combining crosslinking mass-spectrometry, and AlphaFold 2 modeling, we identify the BSE region in Opa1 interacting with the IMS-face of SLC25A46. We observe that this interaction is nucleotide state independent. We also describe interactions between SLC25A46 N-terminal region and the HR1 region of Mfn2. The crosslinked residues K416 and K420 are conserved in Mfn1, suggesting the interaction we see for Mfn2 is also possible for Mfn1.

Our pull-down experiments showed SLC25A46-Mfn2 interaction was maintained despite deletion of the N-terminal region of SLC25A46. In yeast, residues 1-294 of Ugo1 interacts with Fzo1 in a region comprising the transmembrane segments, residues N-terminal to the first transmembrane helix and the C-terminal HR2 (34). From these observations, we speculate that the region downstream of residue 83 in SLC25A46 also interacts with Mfn2 and may involve transmembrane-transmembrane interactions.

Reports from several studies indicate that mitochondrial morphology is sensitive to SLC25A46 levels. Schuettpelz *et al.* reported mitochondrial fragmentation in human fibroblasts and HeLa cells upon SLC25A46 KO (8). In SLC25A46 KO HCT116 cells, we observed mitochondrial fragmentation upon serum starvation. In addition, we observed a ~2-fold slower growth of this cell line, consistent observations in SLC25A46 deleted fibroblasts deletion (8). Overexpression of SLC25A46 in all tested cell lines caused

mitochondrial fragmentation (6, 24, 31). The overexpression findings suggest that at high levels, SLC25A46 can inhibit the activity of the protein fusogens. One possible mode of inhibitory action may be SLC25A46 binding would be sufficient to result in steric competition for Opa1 self-assembly, which relies on the BSE and stalk regions to mediate formation of helical filaments (52-54). Consistent with this prediction, levels of Opa1 oligomeric complexes were found to increase upon loss of SLC25A46 (8).

In our study, SLC25A46 mutants targeting Opa1 interaction did not promote a hyperfused phenotype, but instead disrupted the mitochondrial network. This suggests that a SLC25A46-Opa1 interaction promotes fusion necessary for a tubular network. Although we could not estimate the relative levels of (Δ2-83)SLC25A46, this N-terminal deletion reduced the filamentous network, while increasing the proportion of short tubules, also suggesting a fusion defect. Taken together, these observations provide evidence for SLC25A46 playing an activating role in fusion when expressed at physiological levels.

Our results provide a basis for future functional analyses of the SLC25A46 interaction with the fusion machinery. SLC25A46 protein-protein interactions also may regulate cristae morphology, which is dramatically affected upon loss of SLC25A46 (6, 8, 24, 26, 27, 29). Proteomics studies have also implicated SLC25A46 endoplasmic reticulum interaction partners in maintaining ER-mitochondria contacts facilitating lipid flux (6-8). Future mechanistic structure-activity studies are necessary to explore these other roles of SLC25A46 in cristae regulation and lipid metabolism.

Experimental procedures

Plasmids

Genes for SLC25A46, Mfn2, Opa1(253-960), Opa1(MGD) constructs were synthesized (GenScript) and cloned into pPICZ A for *P. pastoris* expression. C-terminus of SLC25A46 was fused to a $(G_4S)_3$ linker followed by TEV cleavage site and deca-histidine. N-terminus of Opa1(253-960), Opa1(263-960), Opa1(MGD) was tagged with Twin-Strep tag followed by HRV 3C cleavage site and $(G_4S)_3$ linker. C-terminus of Mfn2 was fused to G_3S linker, HRV 3C cleavage site and Twin-Strep tag. For co-expression, SLC25A46 and either Mfn2 or Opa1 with tags with its own AOX1 promoter and terminator were cloned into the same plasmid. Strep-Opa1(253-960) and Strep-Opa1(MGD) were also cloned into pET-28a(+) vector for expression in *E. coli*.

Generation of *Pichia* strains

Expression strains were generated from *Pichia pastoris* strain SMD1163 (*his4 pep4 prb1*) (kind gift from Dr. Tom Rapaport (Harvard Medical School) according to established protocols (55). Plasmids were transformed into SMD1163 by electroporation and grown on YPDS (1% yeast extract, 2% peptone, 2% dextrose, 1 M sorbitol) zeocin (InvivoGen, ant-zn-1p) plates. 7-14 resulting colonies were grown in BMGY (1% yeast extract, 2% peptone, 100 mM potassium phosphate pH 6.0, 1.34% yeast nitrogen base, 4×10^{-5}% biotin, 1% glycerol) and induced in BMMY (replaced glycerol with 0.5% methanol in BMGY). Cultures were screened for protein expression by Western using anti-His, anti-Strep, anti-SLC25A46, anti-Opa1 or anti-Mfn2 antibodies.

Binding experiments using lysates

P. pastoris (1 L) expressing SLC25A46, Opa1, Mfn2 alone or in combination were harvested and cryo-milled using SPEX SamplePrep 6875D Freezer/Mill. For StrepTactin column-binding and elution, milled cells (125 mg) was resuspended in 3 ml of 25 mM HEPES, 150 mM NaCl, pH 8.0 buffer containing 1% GDN and protease inhibitors, tumbled for 1-1:30 h at 4 °C. Suspension was centrifuged at 20,000 for 30 min at 4 °C. Supernatant (100 µl) was incubated with 50 µl of StrepTactin XT 4Flow

high-capacity resin in a spin column (Abcam, ab286861) at 4°C for 15 min followed by centrifugation at 500 xg for 30 s. Resin was washed 3x with 100 µl buffer containing 0.1% GDN. To elute, the resin was incubated with 100 µl buffer with 50 mM biotin for 15 min and centrifuged. Same procedure for Ni-NTA binding experiments except that the binding and elution buffer contained 80 mM and 500 mM imidazole, respectively.

AlphaFold 2 modeling

Protein sequences for human SLC25A46, Opa1 and Mfn2 were run through in a AlphaFold2 Google ColabFold – v 1.5.3 workbook (38, 39, 56). Five independent runs generated the top three ranked relaxed models for SLC25A46-Opa1 and SLC25A46-Mfn2 models respectively.

Data availability

Mass spectrometry data available on request.

Supporting information

This article contains supporting information.

Acknowledgements

We thank Dr. Yuan Gao and Dr. Tom Rapoport for providing *Pichia pastoris* strain SMD1163. We thank all the members of the Chao lab for critical feedback.

Funding and additional information

Mass spectrometric experiments supported by a shared instrumentation grant from the NIH, 1S10OD010582-01A1 towards purchase of Orbitrap Eclipse. This work was supported by funding from the National Institutes of Health (R35GM142553 to L.H.C.)

References

1. Wai, T., andLanger, T. (2016) Mitochondrial Dynamics and Metabolic Regulation Trends Endocrinol Metab **27**, 105-117 10.1016/j.tem.2015.12.001
2. Yapa, N. M. B., Lisnyak, V., Reljic, B., andRyan, M. T. (2021) Mitochondrial dynamics in health and disease FEBS Lett **595**, 1184-1204 10.1002/1873-3468.14077
3. Giacomello, M., Pyakurel, A., Glytsou, C., andScorrano, L. (2020) The cell biology of mitochondrial membrane dynamics Nat Rev Mol Cell Biol **21**, 204-224 10.1038/s41580-020-0210-7
4. Chan, D. C. (2020) Mitochondrial Dynamics and Its Involvement in Disease Annu Rev Pathol **15**, 235-259 10.1146/annurev-pathmechdis-012419-032711
5. Meyer, J. N., Leuthner, T. C., andLuz, A. L. (2017) Mitochondrial fusion, fission, and mitochondrial toxicity Toxicology **391**, 42-53 10.1016/j.tox.2017.07.019
6. Janer, A., Prudent, J., Paupe, V., Fahiminiya, S., Majewski, J., Sgarioto, N. *et al.* (2016) SLC25A46 is required for mitochondrial lipid homeostasis and cristae maintenance and is responsible for Leigh syndrome EMBO Mol Med **8**, 1019-1038 10.15252/emmm.201506159
7. Perivolidi, V. I., Violitzi, F., Ioannidou, E., Rinotas, V., Stamatakis, G., Samiotaki, M. *et al.* (2022) Proteomic Identification of the SLC25A46 Interactome in Transgenic Mice Expressing SLC25A46-FLAG J Proteome Res **21**, 375-394 10.1021/acs.jproteome.1c00728
8. Schuettpelz, J., Janer, A., Antonicka, H., andShoubridge, E. A. (2023) The role of the mitochondrial outer membrane protein SLC25A46 in mitochondrial fission and fusion Life Sci Alliance **6**, 10.26508/lsa.202301914
9. Steffen, J., Vashisht, A. A., Wan, J., Jen, J. C., Claypool, S. M., Wohlschlegel, J. A. *et al.* (2017) Rapid degradation of mutant SLC25A46 by the ubiquitin-proteasome system results in MFN1/2-mediated hyperfusion of mitochondria Mol Biol Cell **28**, 600-612 10.1091/mbc.E16-07-0545
10. Kodal, L. S., Hammer-Hansen, S., Holm-Yildiz, S., Gronskov, K., Karstensen, H. G., andDysgaard, T. (2022) Case report: A novel variant in SLC25A46 causing sensorimotor polyneuropathy and optic atrophy Front Neurol **13**, 1066040 10.3389/fneur.2022.1066040
11. Yamada, M., Suzuki, H., Adachi, H., Noguchi, A., Miya, F., Takahashi, T. *et al.* (2022) Diagnosis of SLC25A46-related pontocerebellar hypoplasia in two siblings with fulminant neonatal course: role of postmortem CT and whole genomic analysis: a case report BMC Neurol **22**, 20 10.1186/s12883-021-02540-x
12. Li, Q., Madden, J. A., Lin, J., Shi, J., Rosen, S. M., Schmitz-Abe, K. *et al.* (2021) Reanalysis of Exome Data Identifies Novel SLC25A46 Variants Associated with Leigh Syndrome J Pers Med **11**, 10.3390/jpm11121277
13. Raju, S., Medarametla, S., andBoraiah, N. (2021) Dystonia and Hereditary Motor Sensory Neuropathy 6B Due to SLC25A46 Gene Mutations Mov Disord Clin Pract **8**, 480-482 10.1002/mdc3.13139
14. Bitetto, G., Malaguti, M. C., Ceravolo, R., Monfrini, E., Straniero, L., Morini, A. *et al.* (2020) SLC25A46 mutations in patients with Parkinson's Disease and optic atrophy Parkinsonism Relat Disord **74**, 1-5 10.1016/j.parkreldis.2020.03.018

15. Abrams, A. J., Fontanesi, F., Tan, N. B. L., Buglo, E., Campeanu, I. J., Rebelo, A. P. *et al.* (2018) Insights into the genotype-phenotype correlation and molecular function of SLC25A46 Hum Mutat **39**, 1995-2007 10.1002/humu.23639
16. Ivanov, I., Atkinson, D., Litvinenko, I., Angelova, L., Andonova, S., Mumdjiev, H. *et al.* (2018) Pontocerebellar hypoplasia type 1 for the neuropediatrician: Genotype-phenotype correlations and diagnostic guidelines based on new cases and overview of the literature Eur J Paediatr Neurol **22**, 674-681 10.1016/j.ejpn.2018.03.011
17. Braunisch, M. C., Gallwitz, H., Abicht, A., Diebold, I., Holinski-Feder, E., Van Maldergem, L. *et al.* (2018) Extension of the phenotype of biallelic loss-of-function mutations in SLC25A46 to the severe form of pontocerebellar hypoplasia type I Clin Genet **93**, 255-265 10.1111/cge.13084
18. van Dijk, T., Rudnik-Schoneborn, S., Senderek, J., Hajmousa, G., Mei, H., Dusl, M. *et al.* (2017) Pontocerebellar hypoplasia with spinal muscular atrophy (PCH1): identification of SLC25A46 mutations in the original Dutch PCH1 family Brain **140**, e46 10.1093/brain/awx147
19. Hammer, M. B., Ding, J., Mochel, F., Eleuch-Fayache, G., Charles, P., Coutelier, M. *et al.* (2017) SLC25A46 Mutations Associated with Autosomal Recessive Cerebellar Ataxia in North African Families Neurodegener Dis **17**, 208-212 10.1159/000464445
20. Sulaiman, R. A., Patel, N., Alsharif, H., Arold, S. T., andAlkuraya, F. S. (2017) A novel mutation in SLC25A46 causes optic atrophy and progressive limb spasticity, with no cerebellar atrophy or axonal neuropathy Clin Genet **92**, 230-231 10.1111/cge.12963
21. Wan, J., Steffen, J., Yourshaw, M., Mamsa, H., Andersen, E., Rudnik-Schoneborn, S. *et al.* (2016) Loss of function of SLC25A46 causes lethal congenital pontocerebellar hypoplasia Brain **139**, 2877-2890 10.1093/brain/aww212
22. Charlesworth, G., Balint, B., Mencacci, N. E., Carr, L., Wood, N. W., andBhatia, K. P. (2016) SLC25A46 mutations underlie progressive myoclonic ataxia with optic atrophy and neuropathy Mov Disord **31**, 1249-1251 10.1002/mds.26716
23. Nguyen, M., Boesten, I., Hellebrekers, D. M., Mulder-den Hartog, N. M., de Coo, I. F., Smeets, H. J. *et al.* (2017) Novel pathogenic SLC25A46 splice-site mutation causes an optic atrophy spectrum disorder Clin Genet **91**, 121-125 10.1111/cge.12774
24. Abrams, A. J., Hufnagel, R. B., Rebelo, A., Zanna, C., Patel, N., Gonzalez, M. A. *et al.* (2015) Mutations in SLC25A46, encoding a UGO1-like protein, cause an optic atrophy spectrum disorder Nat Genet **47**, 926-932 10.1038/ng.3354
25. Kunji, E. R. S., King, M. S., Ruprecht, J. J., andThangaratnarajah, C. (2020) The SLC25 Carrier Family: Important Transport Proteins in Mitochondrial Physiology and Pathology Physiology (Bethesda) **35**, 302-327 10.1152/physiol.00009.2020
26. Duchesne, A., Vaiman, A., Castille, J., Beauvallet, C., Gaignard, P., Floriot, S. *et al.* (2017) Bovine and murine models highlight novel roles for SLC25A46 in mitochondrial dynamics and metabolism, with implications for human and animal health PLoS Genet **13**, e1006597 10.1371/journal.pgen.1006597

27. Li, Z., Peng, Y., Hufnagel, R. B., Hu, Y. C., Zhao, C., Queme, L. F. *et al.* (2017) Loss of SLC25A46 causes neurodegeneration by affecting mitochondrial dynamics and energy production in mice Hum Mol Genet **26**, 3776-3791 10.1093/hmg/ddx262
28. Suda, K., Ueoka, I., Azuma, Y., Muraoka, Y., Yoshida, H., andYamaguchi, M. (2018) Novel Drosophila model for mitochondrial diseases by targeting of a solute carrier protein SLC25A46 Brain Res **1689**, 30-44 10.1016/j.brainres.2018.03.028
29. Terzenidou, M. E., Segklia, A., Kano, T., Papastefanaki, F., Karakostas, A., Charalambous, M. *et al.* (2017) Novel insights into SLC25A46-related pathologies in a genetic mouse model PLoS Genet **13**, e1006656 10.1371/journal.pgen.1006656
30. Qiu, K., Zou, W., Fang, H., Hao, M., Mehta, K., Tian, Z. *et al.* (2022) Light-activated mitochondrial fission through optogenetic control of mitochondria-lysosome contacts Nat Commun **13**, 4303 10.1038/s41467-022-31970-5
31. Santo-Domingo, J., Lassueur, S., Galindo, A. N., Alvarez-Illera, P., Romero-Sanz, S., Caldero-Escudero, E. *et al.* (2023) SLC25A46 promotes mitochondrial fission and mediates resistance to lipotoxic stress in INS-1E insulin-secreting cells J Cell Sci **136**, 10.1242/jcs.260049
32. Coonrod, E. M., Karren, M. A., andShaw, J. M. (2007) Ugo1p is a multipass transmembrane protein with a single carrier domain required for mitochondrial fusion Traffic **8**, 500-511 10.1111/j.1600-0854.2007.00550.x
33. Sesaki, H., andJensen, R. E. (2001) UGO1 encodes an outer membrane protein required for mitochondrial fusion J Cell Biol **152**, 1123-1134 10.1083/jcb.152.6.1123
34. Sesaki, H., andJensen, R. E. (2004) Ugo1p links the Fzo1p and Mgm1p GTPases for mitochondrial fusion J Biol Chem **279**, 28298-28303 10.1074/jbc.M401363200
35. Hoppins, S., Horner, J., Song, C., McCaffery, J. M., andNunnari, J. (2009) Mitochondrial outer and inner membrane fusion requires a modified carrier protein J Cell Biol **184**, 569-581 10.1083/jcb.200809099
36. Sesaki, H., Southard, S. M., Yaffe, M. P., andJensen, R. E. (2003) Mgm1p, a dynamin-related GTPase, is essential for fusion of the mitochondrial outer membrane Mol Biol Cell **14**, 2342-2356 10.1091/mbc.e02-12-0788
37. Wong, E. D., Wagner, J. A., Scott, S. V., Okreglak, V., Holewinske, T. J., Cassidy-Stone, A. *et al.* (2003) The intramitochondrial dynamin-related GTPase, Mgm1p, is a component of a protein complex that mediates mitochondrial fusion J Cell Biol **160**, 303-311 10.1083/jcb.200209015
38. Jumper, J., Evans, R., Pritzel, A., Green, T., Figurnov, M., Ronneberger, O. *et al.* (2021) Highly accurate protein structure prediction with AlphaFold Nature **596**, 583-589 10.1038/s41586-021-03819-2
39. Mirdita, M., Schutze, K., Moriwaki, Y., Heo, L., Ovchinnikov, S., andSteinegger, M. (2022) ColabFold: making protein folding accessible to all Nat Methods **19**, 679-682 10.1038/s41592-022-01488-1

40. Ishihara, N., Fujita, Y., Oka, T., andMihara, K. (2006) Regulation of mitochondrial morphology through proteolytic cleavage of OPA1 EMBO J **25**, 2966-2977 10.1038/sj.emboj.7601184
41. Olichon, A., Emorine, L. J., Descoins, E., Pelloquin, L., Brichese, L., Gas, N. *et al.* (2002) The human dynamin-related protein OPA1 is anchored to the mitochondrial inner membrane facing the inter-membrane space FEBS Lett **523**, 171-176 10.1016/s0014-5793(02)02985-x
42. Chappie, J. S., Acharya, S., Liu, Y. W., Leonard, M., Pucadyil, T. J., andSchmid, S. L. (2009) An intramolecular signaling element that modulates dynamin function in vitro and in vivo Mol Biol Cell **20**, 3561-3571 10.1091/mbc.e09-04-0318
43. Sever, S., Muhlberg, A. B., andSchmid, S. L. (1999) Impairment of dynamin's GAP domain stimulates receptor-mediated endocytosis Nature **398**, 481-486 10.1038/19024
44. Anand, R., Eschenburg, S., andReubold, T. F. (2016) Crystal structure of the GTPase domain and the bundle signalling element of dynamin in the GDP state Biochem Biophys Res Commun **469**, 76-80 10.1016/j.bbrc.2015.11.074
45. Chappie, J. S., Acharya, S., Leonard, M., Schmid, S. L., andDyda, F. (2010) G domain dimerization controls dynamin's assembly-stimulated GTPase activity Nature **465**, 435-440 10.1038/nature09032
46. Kong, L., Sochacki, K. A., Wang, H., Fang, S., Canagarajah, B., Kehr, A. D. *et al.* (2018) Cryo-EM of the dynamin polymer assembled on lipid membrane Nature **560**, 258-262 10.1038/s41586-018-0378-6
47. Gao, S., andHu, J. (2021) Mitochondrial Fusion: The Machineries In and Out Trends Cell Biol **31**, 62-74 10.1016/j.tcb.2020.09.008
48. Anand, R., Wai, T., Baker, M. J., Kladt, N., Schauss, A. C., Rugarli, E. *et al.* (2014) The i-AAA protease YME1L and OMA1 cleave OPA1 to balance mitochondrial fusion and fission J Cell Biol **204**, 919-929 10.1083/jcb.201308006
49. Ban, T., Ishihara, T., Kohno, H., Saita, S., Ichimura, A., Maenaka, K. *et al.* (2017) Molecular basis of selective mitochondrial fusion by heterotypic action between OPA1 and cardiolipin Nat Cell Biol **19**, 856-863 10.1038/ncb3560
50. Ge, Y., Shi, X., Boopathy, S., McDonald, J., Smith, A. W., andChao, L. H. (2020) Two forms of Opa1 cooperate to complete fusion of the mitochondrial inner-membrane Elife **9**, 10.7554/eLife.50973
51. Mishra, P., Carelli, V., Manfredi, G., andChan, D. C. (2014) Proteolytic cleavage of Opa1 stimulates mitochondrial inner membrane fusion and couples fusion to oxidative phosphorylation Cell Metab **19**, 630-641 10.1016/j.cmet.2014.03.011
52. Faelber, K., Dietrich, L., Noel, J. K., Wollweber, F., Pfitzner, A. K., Muhleip, A. *et al.* (2019) Structure and assembly of the mitochondrial membrane remodelling GTPase Mgm1 Nature **571**, 429-433 10.1038/s41586-019-1372-3
53. Nyenhuis, S. B., Wu, X., Strub, M. P., Yim, Y. I., Stanton, A. E., Baena, V. *et al.* (2023) OPA1 helical structures give perspective to mitochondrial dysfunction Nature **620**, 1109-1116 10.1038/s41586-023-06462-1
54. von der Malsburg, A., Sapp, G. M., Zuccaro, K. E., von Appen, A., Moss, F. R., 3rd, Kalia, R. *et al.* (2023) Structural mechanism of mitochondrial membrane

remodelling by human OPA1 Nature **620**, 1101-1108 10.1038/s41586-023-06441-6

55. Hartmann, L., Kugler, V., andWagner, R. (2016) Expression of Eukaryotic Membrane Proteins in Pichia pastoris Methods Mol Biol **1432**, 143-162 10.1007/978-1-4939-3637-3_10

56. https://colab.research.google.com/github/deepmind/alphafold/blob/main/notebooks/AlphaFold.ipynb

57. Wang, R., Mishra, P., Garbis, S. D., Moradian, A., Sweredoski, M. J., andChan, D. C. (2021) Identification of new OPA1 cleavage site reveals that short isoforms regulate mitochondrial fusion Mol Biol Cell **32**, 157-168 10.1091/mbc.E20-09-0605

58. Schindelin, J., Arganda-Carreras, I., Frise, E., Kaynig, V., Longair, M., Pietzsch, T. *et al.* (2012) Fiji: an open-source platform for biological-image analysis Nat Methods **9**, 676-682 10.1038/nmeth.2019

Abbreviations and nomenclature

OMM – outer mitochondrial membrane
IMM – inner mitochondrial membrane
SLC – solute carrier family
SLC25A46 – solute carrier family 25 member A46
Opa1 – optic atrophy 1
Mfn1/2 – mitofusin 1/2
iPSC – induced pluoripotent stem cells
BSE – bundle signaling element
HR1/2 – heptad repeat 1/2
ER – endoplasmic reticulum
MGD – minimal GTPase domain
DDM – n-Dodecyl-β-D-Maltopyranoside
GDN – glyco-diosgenin
PA – phosphatidic acid
TM – transmembrane segment
MTS – mitochondrial targeting sequence
IMS – inter-membrane space

Figure legends

Figure 1. SLC25A46 interacts with the bundle signaling element (BSE) of Opa1.

A. Domain diagrams of SLC25A46 and Opa1. s-Opa1 (amino acids 253-960) used in this study is designated below full length Opa1 sequence.

B. GDN extracts prepared from *P. pastoris* expressing SLC25A46-His, Strep-Opa1 or co-expressing SLC25A46-His and Strep-Opa1 subjected to StrepTactin column binding and elution.

C. Crosslinks identified in BSE helices 2 and 3 of Opa1. Circular map of SLC25A46 and Opa1 with identified lysine-lysine crosslinks (black arcs). Crosslinker used to generate the crosslink is indicated.

D. AlphaFold 2 model of the SLC25A46-Opa1 interaction. N-terminal region of SLC25A46 comprising residues 1-83 (disordered) not displayed, residues 1-263 of Opa1 not modeled. Box region displaying identified crosslinks and the calculated C□-C□ distances based on the model.

Figure 2. SLC25A46 mutations in the binding interface diminish binding to Opa1.

A. Mutations designed to disrupt the interaction are mapped on the AlphaFold 2 model of the SLC25A46-Opa1 complex. Box enlarged and depicted in open book format.

B. Purified SLC25A46-His WT, I349D mutant or R257A/R347A double mutant were incubated with 2 µM of Strep-Opa1 and subjected to StrepTactin binding and elution experiments. Input and elution analyzed by Western blotting.

Figure 3. The BSE of Opa1 in sufficient to bind SLC25A46.

A. Domain diagrams of SLC25A46 and Opa1. Minimal GTPase domain of Opa1 designated Opa1(MGD) is composed of the GTPase domain and three BSE helices, shown as line diagram below full length Opa1 sequence.

B. Purified SLC25A46-His WT was incubated with 2 µM of Strep-Opa1 or Strep-Opa1(MGD) and subjected to StrepTactin binding and elution. Input and elution analyzed by Western blotting. Control reaction: 10 µM of SLC25A46-His alone.

C. Circular map of SLC25A46 and Opa1(MGD) with identified lysine-lysine crosslinks (black arcs) shown. Crosslinker used is indicated. Crosslinks were identified in BSE helices 2 and 3 of Opa1(MGD) as in Opa1.

D. A model of the SLC25A46-Opa1(MGD) interaction. The N-terminal region of SLC25A46 (residues 1-83) is disordered and not displayed. Boxed region enlarged on right displaying the identified crosslinks and the calculated C□-C□ distances based on the model.

Figure 4. Disease-causing SLC25A46 mutants retain binding to Opa1 or Mfn2.

A. Identified SLC25A46 disease mutations mapped on AlphaFold 2 model of SLC25A46-Opa1 complex. Box regions enlarged on the right to display the mutations.

B. GDN extracts from *P. pastoris* co-expressing Strep-Opa1 and SLC25A46-His WT or mutants subjected to StrepTactin (middle) or Ni-NTA (bottom) column binding and elution.

Figure 5. Mutations disrupting Opa1 interaction alters mitochondrial morphology.

A. Western blot of expression levels for Opa1, Mfn2, SLC25A46 or MTCO1 in HCT116 WT, SLC25A46-KO or SLC25A46-KO cells expressing SLC25A46 variants. (Δ2-

83)SLC25A46 not detected as commercially available antibodies detect the N-terminal epitope of SLC25A46. MTCO1 is used as loading control.

B. Mitochondrial morphology in HCT116 WT, SLC25A46-KO or SLC25A46-KO cells expressing SLC25A46 variants. Mitochondrial morphology for 100 cells were scored for each condition and evaluated (see Materials and Methods).

Figure 1

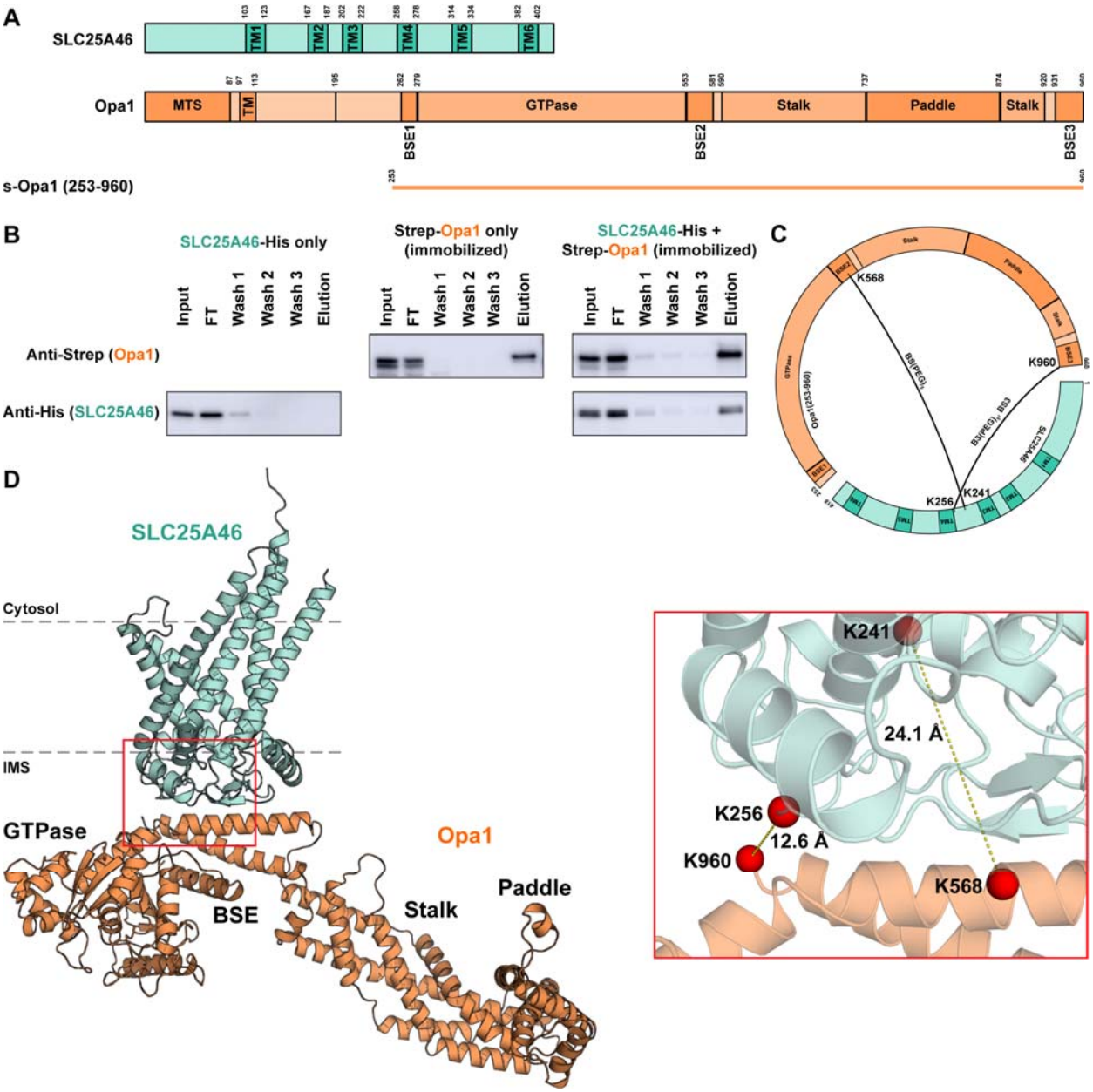
A
SLC25A46
TM1
TM2
TM3
TM4
TM5
TM6
Opa1
MTS
TM
GTPase
Stalk
Paddle
Stalk
BSE1
BSE2
BSE3
s-Opa1 (253-960)
B
SLC25A46-His only
Strep-Opa1 only (immobilized)
SLC25A46-His + Strep-Opa1 (immobilized)
Input
FT
Wash 1
Wash 2
Wash 3
Elution
Anti-Strep (Opa1)
Anti-His (SLC25A46)
C
K568
K960
K256
K241
D
SLC25A46
Cytosol
IMS
GTPase
Opa1
BSE
Stalk
Paddle
K241
24.1 Å
K256
12.6 Å
K960
K568

Figure 2

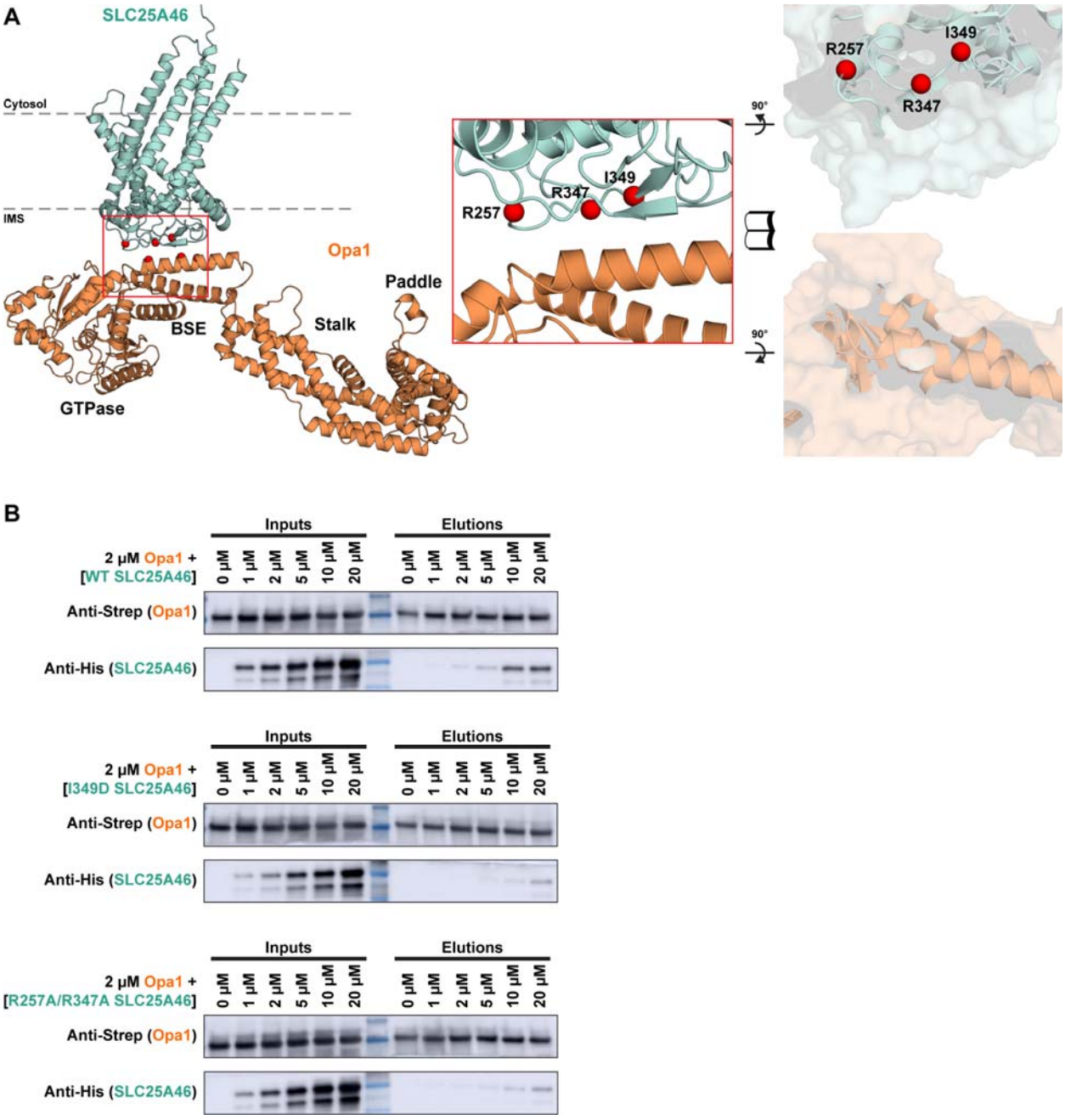
A
SLC25A46
Cytosol
IMS
Opa1
Paddle
BSE
Stalk
GTPase
R257
R347
I349
90°
B
Inputs
Elutions
2 μM Opa1 +
[WT SLC25A46]
[I349D SLC25A46]
[R257A/R347A SLC25A46]
0 μM
1 μM
2 μM
5 μM
10 μM
20 μM
Anti-Strep (Opa1)
Anti-His (SLC25A46)

Figure 3

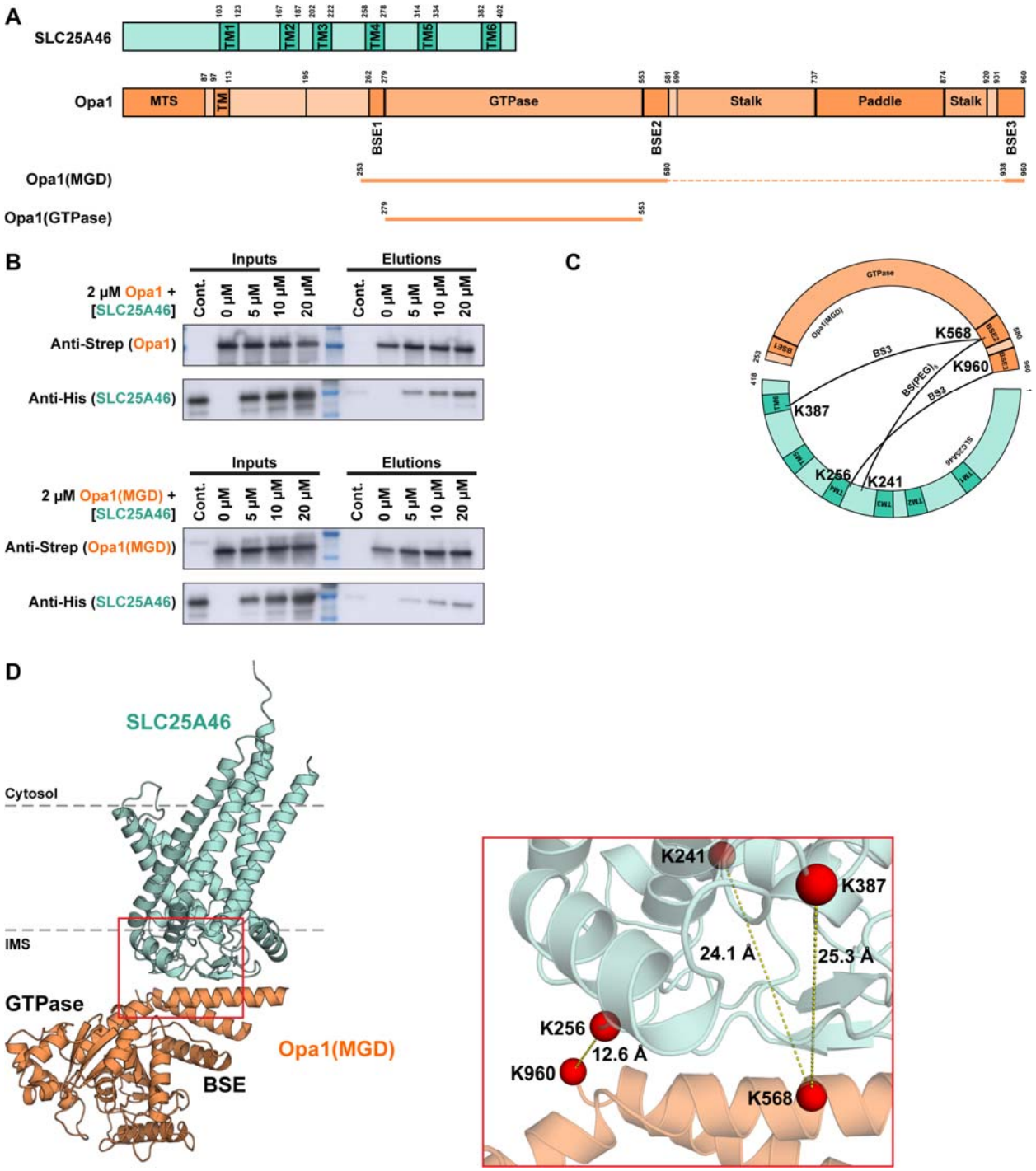
A
SLC25A46
TM1
TM2
TM3
TM4
TM5
TM6
Opa1
MTS
TM
GTPase
Stalk
Paddle
Stalk
BSE1
BSE2
BSE3
Opa1(MGD)
Opa1(GTPase)
B
Inputs
Elutions
2 μM Opa1 + [SLC25A46]
Cont.
0 μM
5 μM
10 μM
20 μM
Anti-Strep (Opa1)
Anti-His (SLC25A46)
2 μM Opa1(MGD) + [SLC25A46]
Anti-Strep (Opa1(MGD))
C
K568
K960
K387
K256
K241
BS3
BS(PEG)5
D
SLC25A46
Cytosol
IMS
GTPase
Opa1(MGD)
BSE
K241
K387
24.1 Å
25.3 Å
K256
12.6 Å
K960
K568

Figure 4

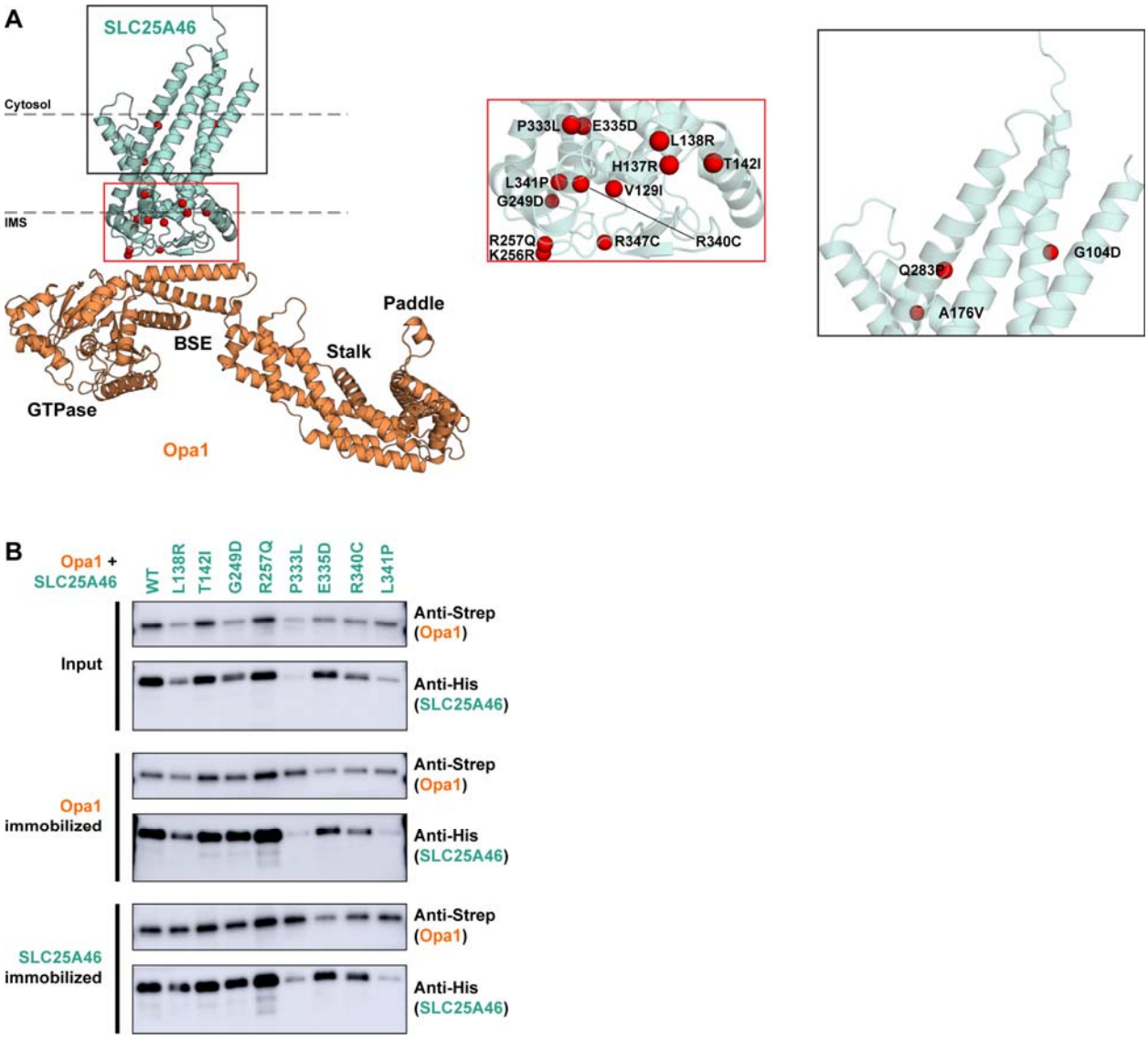
A
SLC25A46
Cytosol
IMS
Paddle
BSE
Stalk
GTPase
Opa1
P333L
E335D
L138R
H137R
T142I
L341P
V129I
G249D
R257Q
K256R
R347C
R340C
G104D
Q283E
A176V
B
Opa1 +
SLC25A46
WT
L138R
T142I
G249D
R257Q
P333L
E335D
R340C
L341P
Input
Opa1
immobilized
SLC25A46
immobilized
Anti-Strep
(Opa1)
Anti-His
(SLC25A46)

Figure 5

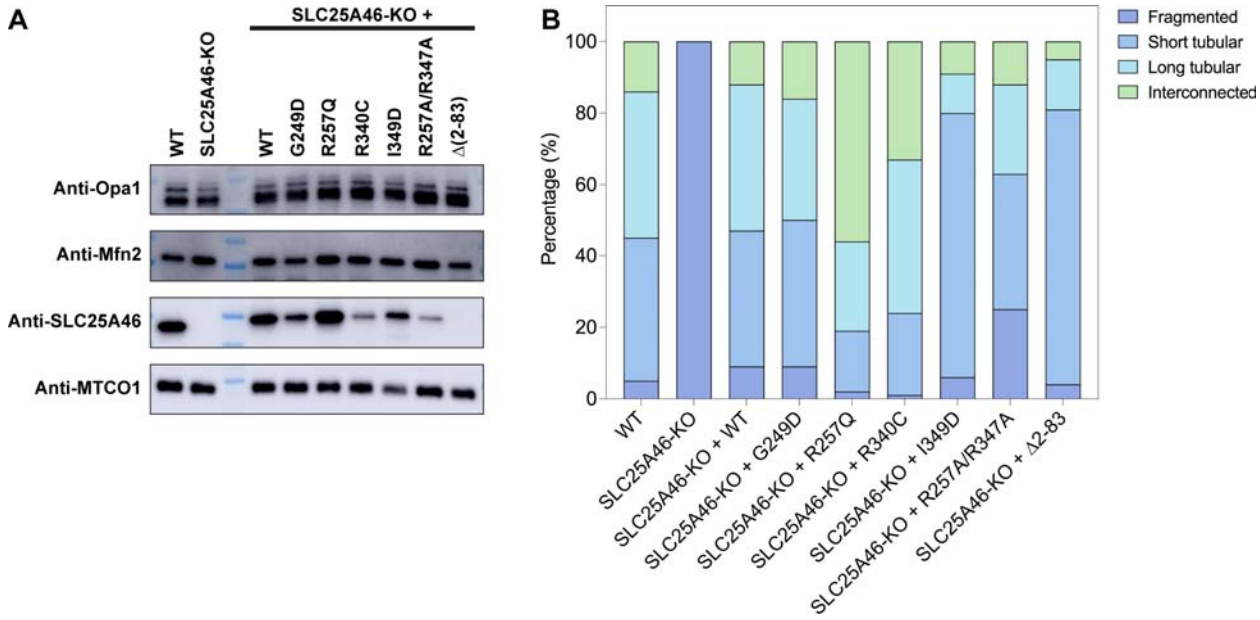
A
SLC25A46-KO +
WT
SLC25A46-KO
WT
G249D
R257Q
R340C
I349D
R257A/R347A
Δ(2-83)
Anti-Opa1
Anti-Mfn2
Anti-SLC25A46
Anti-MTCO1
B
Percentage (%)
100
80
60
40
20
0
Fragmented
Short tubular
Long tubular
Interconnected
WT
SLC25A46-KO
SLC25A46-KO + WT
SLC25A46-KO + G249D
SLC25A46-KO + R257Q
SLC25A46-KO + R340C
SLC25A46-KO + I349D
SLC25A46-KO + R257A/R347A
SLC25A46-KO + Δ2-83

Supporting Information

Supporting experimental procedures

Binding experiments using lysates – additional details

For nucleotide treatments, StrepTactin binding experiments were performed as described but the buffer used was 25 mM HEPES, 100 mM NaCl, 50 mM KCl, 10 mM $MgCl_2.6H_2O$, pH 8.0, 1% GDN (extraction) or 0.1% GDN (binding and elution) and containing 2 mM of GTPγS (Sigma-Aldrich, 10220647001), GMPPCP (Sigma-Aldrich, M3509-25MG) or GDP (Sigma-Aldrich, G7127-25MG).

To assess binding of SLC25A46-His disease mutants to Opa1 or Mfn2, *P. pastoris* strains co-expressing the proteins were cultured in 5-10 ml BMMY. Equal number of cells (estimated by OD600) were harvested from each culture. The cells were resuspended in 0.5 ml of 25 mM HEPES, 150 mM NaCl, pH 8.0 containing protease inhibitors. An equal volume of 0.5 mm glass beads was added and lysed using a Retsch TissueLyzer. To the recovered lysate, GDN was added from a stock solution of 10% to a final concentration of 1% and incubated in the cold room for 1.5 h tumbling gently. The lysate was then centrifuged at 21,100 xg for 30 min at 4 °C. 150-300 ul of the lysate was applied to either Ni-NTA (Bio-Rad, 780-0800) or StrepTactin XT 4Flow resin pre-equilibrated with the above buffer containing 10 mM imidazole (for Ni-NTA) or 1 mM EDTA (StrepTactin) and 0.1% GDN. Resins were washed 3x and eluted with buffer containing 500 mM imidazole (for Ni-NTA) or 50 mM biotin (StrepTactin) and 0.1% GDN. The samples were subjected to western blotting using anti-Strep (Mfn2 or Opa1) and anti-His (SLC25A46) antibodies.

Protein expression

For protein expression in *P. pastoris*, a single desired clone was inoculated in 5-10 ml BMGY and then scaled up to 500 ml BMGY media and grown overnight at 30 °C. The culture was harvested and resuspended in 6 litres BMMY at an OD600 of 1.0 for protein induction. The induced cultures were then grown at 20 °C and harvested 24 h later. Cell pellets were frozen in liquid nitrogen and stored at –80 °C.

Opa1 and Opa1(MGD) were also purified from *E. coli*. For expression in *E. coli*, transformed BL21-CodonPlus (DE3)-RIL cells (Agilent, 230245) were grown in LB at 37 °C to an OD600 of 0.7 and induced with 0.2 mM IPTG (Gold Biotechnology, I2481C200) and grown overnight at 16 °C. Cultures were harvested and stored at –80 °C until use.

Purification of SLC25A46

Harvested *P. pastoris* cells expressing WT, I349D mutant or R257A/R347A double mutant were milled under cryogenic conditions using SPEX SamplePrep 6875D Freezer/Mill. All purification steps were done at 4 °C. The milled cells were resuspended in 50 mM HEPES, 250 mM NaCl, 50 mM imidazole, pH 7.8 containing protease inhibitors (Sigma-Aldrich, 5056489001) and benzonase nuclease (Sigma-Aldrich, E1014-25KU). The suspension was centrifuged at 235,000 xg for 0:45 h to collect the insoluble pellet. The pellet was then solubilized in the same buffer containing 2% n-Dodecyl-β-D-Maltopyranoside (DDM) (Anatrace, D310) and stirred for 1 h. The extract was centrifuged at 100,000 xg for 1 h and the supernatant was loaded on Ni-NTA Agarose resin (Qiagen, 30230) pre-equilibrated with 25 mM HEPES, 150 mM NaCl, 50 mM imidazole, pH 7.8, 0.05-0.1% glyco-diosgenin (GDN) (Anatrace, GDN101). The resin was washed with this buffer before elution using buffer containing 500 mM imidazole. The elution fractions were concentrated using 50,000 MWCO concentrators and dialyzed using 20,000 MWCO cassettes (Thermo Fisher Scientific, A52976) against 25 mM HEPES, 150 mM NaCl, pH 8.0, 0.05% GDN. The dialyzed sample was collected and concentrated (50,000 MWCO) further. Protein concentration was estimated by absorbance at 280 nm.

Purification of Opa1 and Opa1(MGD)

All steps were done at 4 °C. Harvested *E. coli* cells expressing Opa1(253-960) or Opa1(MGD) were resuspended in 50 mM HEPES, 250 mM NaCl, 1 mM EDTA, pH 8.0, 1 mg/ml lysozyme, protease inhibitors and benzonase nuclease. The cell suspension was lysed by sonication and centrifuged at 30,000 xg for 1 h. The supernatant was flowed over StrepTactin XT 4Flow high-capacity resin (IBA Lifesciences, 2-5030-010) packed in a gravity column and equilibrated with 25 mM HEPES, 150 mM NaCl, pH 8.0.

The same buffer was used to wash the resin and the bound protein was eluted using buffer containing 50 mM biotin (IBA Lifesciences, 2-1016-005). The fractions were concentrated (50,000 MWCO for Opa1, 20,000 MWCO for Opa1(MGD)) and dialyzed (20,000 MWCO) against 25 mM HEPES, 150 mM NaCl, pH 8.0. The concentrations were estimated using absorbance at 280 nm. The proteins were aliquoted and frozen in liquid nitrogen and stored at -80 °C.

Generation of SLC25A46-Opa1 and SLC25A46-Mfn2 complexes

All purification steps were performed at 4 °C or on ice. To purify SLC25A46-Opa1 complex, *P. pastoris* co-expressing SLC25A46-His and Strep-Opa1 was harvested and cryo-milled as before. The milled cells were resuspended in 25 mM HEPES, 150 mM NaCl, 25 mM imidazole, pH 8.0 containing protease inhibitors and benzonase nuclease. GDN (2%) and 18:1 PA (Avanti Polar Lipids, 840875) (0.1 mg/ml solubilized in GDN) were added and stirred for 2 h. The suspension was centrifuged at 100,000 xg for 1 h. The supernatant was loaded onto a 1 ml HisTrap HP column and washed with 25 mM HEPES, 150 mM NaCl, 25 mM imidazole, pH 8.0, 0.025 mg/ml 18:1 PA and 0.1% GDN and eluted with the same buffer containing 500 mM imidazole. The elution was diluted with StrepTactin binding buffer, 25 mM HEPES, 150 mM NaCl, 1 mM EDTA, pH 8.0, 0.025 mg/ml PA, 0.1% GDN to bring the imidazole concentration below 100 mM and added to 1 ml StrepTactin XT 4Flow resin, washed with the above binding buffer and eluted in buffer containing 50 mM biotin. The elution fractions containing SLC25A46 and Opa1 were combined and concentrated (50,000 MWCO) to ~5.5 mg/ml.

To purify SLC25A46-Mfn2 complex, *P. pastoris* co-expressing SLC25A46-His and Mfn2-Strep was harvested, cryo-milled and resuspended in 25 mM HEPES, 150 mM NaCl, 25 mM imidazole, pH 8.0 with protease inhibitors and benzonase nuclease and centrifuged at 235,000 xg for 45 min to collect the membrane fractions. The membrane fractions were resuspended in the same buffer containing 2% GDN and 0.1 mg/ml PA and stirred for 2 h. The extract was centrifuged and processed using Ni-NTA and StrepTactin columns as described above. The elution fractions from StrepTactin column were concentrated (50,000 MWCO) to ~2.4 mg/ml.

Binding experiments using purified proteins

Binding reactions were prepared in 25 mM HEPES, 150 mM NaCl, pH 8.0, 0.1% GDN (binding buffer). Purified Opa1 at 2 µM concentration was incubated with varying concentrations of SLC25A46 at 4 °C for 3 h. The reaction mixtures (100 µl) were added to 50 µl StrepTactin XT 4Flow high-capacity resin packed in spin column and incubated with gentle agitation for 15 min. The spin columns were centrifuged at 500 xg for 30 s to collect the flow-through. The columns were washed thrice with 100 µl of binding buffer. The bound proteins were eluted by incubating with 100 µl of buffer containing 50 mM biotin for 15 min followed by centrifugation at 500 xg for 30 s. Samples analyzed by Western blotting.

Western blotting

Following SDS PAGE, proteins were transferred to PVDF membrane (Bio-Rad, 1704156) using Bio-Rad Trans-Blot Turbo Transfer system. The membranes were incubated with the primary antibodies as indicated and were probed with the appropriate secondary antibodies conjugated to horseradish peroxidase. The blots were developed using Western Lightning Plus Chemiluminescent Substrate (Revvity, NEL105001EA) and imaged using Amersham Imager 680. Densitometry was performed using ImageJ. Antibodies: anti-His (Thermo Fisher Scientific, MA1-21315, 1:1000), anti-Strep (IBA Lifesciences, 2-1509-001, ~1:33000), anti-SLC25A46 (Abcam, ab237760, 1:2500), anti-Opa1 (Novus Biologicals, NBP2-59770, 1:1000), anti-Mfn2 (Thermo Fisher Scientific, 702768, 1:1000), anti-MTCO1 (Abcam, ab14705, 1:2000), anti-mouse, HRP conjugated (Sigma-Aldrich, GENA931-1ML, 1:5000), anti-rabbit, HRP conjugated (Sigma-Aldrich, GENA934-1ML, 1:5000).

Crosslinking mass spectrometry

For crosslinking, BS3 (Thermo Fisher Scientific, A39266) was added to the concentrated SLC25A46-Opa1(263-960) and SLC25A46-Mfn2 complexes at a final concentration of 0.75 mM. Reactions were incubated on ice for 1 h and quenched by adding Tris-HCl, pH 7.8 at a final concentration of ~45 mM) and incubating 15 min on

ice. The samples were separated on a 7.5% polyacrylamide gel and bands excised for mass spectrometry.

While we identified several monolinks and intralinks in Opa1 with BS3 crosslinker, we were unable to identify any crosslinks with SLC25A46 as the sequencing depth for SLC25A46 in this sample was poor. To overcome this, we performed crosslinking experiments with excess purified proteins. We used $BS(PEG)_5$ (Thermo Fisher Scientific, 21581) (25 mM stock in 10% DMSO) in addition. The crosslinker (BS3 or BS(PEG)5) was added at a final concentration of 2.5 mM to 20 µM SLC25A46 and 30 µM Opa1(253-960) or Opa1(MGD) and the sample separated on a 12% Bis-Tris 1.0 mm, Mini Protein Gels. The subsequent steps were same as above. The excised gel bands were destained with 1:1 v/v methanol and 100 mM ammonium bicarbonate. Gel pieces were partially dehydrated with acetonitrile then further dehydrated by SpeedVac. Proteins were reduced at 57 ˚C for 1 h by adding 100 µl of 20 mM aqueous DTT solution to the dehydrated gel piece. The solution was removed and replaced with 100 µl of a 50 mM iodoacetamide solution and the gel pieces incubated in the dark for 45 min. the solution was removed, and the gel pieces again partially dehydrated with an acetonitrile rinse and further dried in a SpeedVac. 250 ng of sequencing grade modified trypsin (Promega) was added to each sample followed by 300 µl of 100 mM ammonium bicarbonate to cover the gel pieces. Digestion was allowed to proceeded overnight on a shaker at room temperature. To stop the digestion and assist with peptide extraction a solution of 5% formic acid in acetonitrile 1:2 (v:v) was added and incubated for 15 min with agitation. The solution was transferred into a new tube and the procedure repeated two more times. The combined solutions were dried down in a SpeedVac concentrator to remove the acetonitrile. The samples resuspended in 0.1% acetic acid and loaded onto equilibrated Ultra-Micro SpinColumns™ (Harvard Apparatus) using a microcentrifuge. The spin columns were washed three times with 0.1% trifluoroacetic acid and the last wash with 0.5% acetic acid. Peptides were eluted with 40% acetonitrile in 0.5% acetic acid, followed by 80% acetonitrile in 0.5% acetic acid. The solutions combined and dried down using a SpeedVac concentrator. The samples were reconstituted in 0.5% acetic acid and stored at -80 °C until analysis.

Approximately 1 µg of each sample was analyzed individually by LC/MS/MS. Samples were loaded onto an Acclaim PepMap trap column (2 cm x 75 µm) in line with an EASY-Spray analytical column (50 cm x 75 µm ID PepMap C18, 2 µm bead size) using the autosampler of an EASY-nLC 1200 HPLC (Thermo Scientific). Solvent A was 2% acetonitrile in 0.5% acetic acid and solvent B was 80% acetonitrile in 0.5% acetic acid. The gradient used was the following: 5 min held at 5% solvent B, in 60 min to 35% solvent B, in 10 min to 45% solvent B, and in 10 min to 100% solvent B. Peptides were gradient eluted directly into a Thermo Scientific Orbitrap Eclipse Mass Spectrometer.

Mfn2 and SLC25A46 Crosslink analysis:

High resolution full spectra were acquired with a resolution of 240,000, an AGC target of 1e6, with a maximum ion time of 50 ms, and a scan range of 400 to 1500 m/z. All precursors with charge states between 2-7 were selected for fragmentation with a dynamic exclusion of 20 sec. All MS/MS HCD spectra were collected in the ion trap using the rapid scan mode, an AGC target of 2e4, maximum inject time of 18 ms, one microscan, 0.7 m/z isolation window, and normalized collision energy (NCE) of 27. The instrument was set to run at top speed with a cycle time of 3 sec. Samples were run a second time to specifically only fragment precursor ions that are likely crosslinked (charge state 4-10) using either HCD or ETD fragmentation. The gradient used was the following: 5 min held at 5% solvent B, in 120 min to 35% solvent B, in 10 min to 45% solvent B, and in 10 min to 100% solvent B. High resolution full spectra were acquired with a resolution of 60,000, an AGC target of 4e5, with a maximum ion time of 50 ms, and a scan range of 400 to 1500 m/z. Charge states 4-6 were analyzed in the Orbitrap using HCD with an NCE of 27, resolution of 30K, AGC target of 2e5, maximum inject time of 200 msec and an isolation window of 2. Charge states 7-10 were analyzed in the Orbitrap using ETD with a charge state dependent reaction time, resolution of 30K, AGC target of 2e5, maximum inject time of 54 msec and an isolation window of 2.

Opa1 and SLC25A46 Crosslink analysis:

High resolution full spectra were acquired with a resolution of 120,000, an AGC target of 4e6, with a maximum ion time of 50 ms, and a scan range of 400 to 1500 m/z. All precursors with charge states between 2-5 were selected for fragmentation with a dynamic exclusion of 30 sec. All MS/MS HCD spectra were collected in the Orbitrap

with a resolution of 30K, an AGC target of 2e5, maximum inject time of 200 ms, one microscan, 2 m/z isolation window, and normalized collision energy (NCE) of 27. MS/MS spectra were searched in Byos by Protein Metrics against the human SLC25A46, Opa1 and Mfn2 sequences to identify crosslinked peptides.

Cell lines and culture conditions

HCT116 WT and SLC25A46 KO cells were kind gifts from CeMM (Research Center for Molecular Medicine, Medical University of Vienna, Austria). The cells maintained in RPMI 1640 with 10% fetal bovine serum (FBS) and 1% penicillin/streptomycin at 37 °C and 5% CO_2. Cell genotype confirmed by Western blotting. Human SLC25A46 sequence from plasmid pDONR221_SLC25A46 (a gift from RESOLUTE Consortium & Giulio Superti-Furga (Addgene plasmid #131971; http://n2t.net/addgene:131971; RRID:Addgene_131971) was cloned into pCDNA3.1(+) plasmid to generate the construct pAH9. Site-directed mutagenesis (New England Biolabs) was used to generate expression plasmids bearing the mutations G249D (pAH10), R257Q (pAH11), R340C (pAH12), I349D (pAH13), Δ1-83 (pAH14) and R257A/R347A (pAH36) in the SLC25A46 coding sequence of pAH9. To transiently express SLC25A46 and its mutant derivatives in HCT116 SLC25A46 KO cells, cells seeded onto 35 mm glass-bottom dishes (MatTek Life Sciences) coated with poly-D-lysine (0.1 mg/ml) were transfected with 2.5 µg expression plasmid mixed with Lipofectamine 3000 in a total volume of 250 µl Opti-MEM (Thermo Fisher Scientific). Cells were grown for 36-48 h prior to imaging.

For Western blotting, mitochondria were isolated using Qiagen Qproteome Mitochondria Isolation Kit (Qiagen, 37612). Protease inhibitors were added to isolated mitochondria and solubilized using 0.5% DDM. Protein content was estimated using Bradford assay (Bio-Rad, 5000205). ~1 µg of total protein was loaded on.

Fluorescence imaging and quantification

HCT116 cells were seeded onto glass-bottom dishes and grown to ~80% confluency. Cells were washed with PBS and fixed in 4% paraformaldehyde (PFA) in PBS for 20 min. Following three PBS washes, cells were permeabilized in 0.1% Triton

X-100 diluted in PBS for 5 min. Cells were incubated in 2% normal goat serum and 0.05% Triton X-100 in PBS for 1 h, then incubated in the same buffer with 1:300 Tom20 rabbit antibody (Invitrogen, MAS-34964) for 1 h at room temperature or overnight at 4˚C. After 3 washes with PBS, cells were incubated with 1:1000 goat anti-rabbit Alexa Fluor® 488 AffiniPure antibody (Jackson ImmunoResearch, 111-545-144) for 1 h at room temperature. Cells were washed in PBS and coated with UltraCruz® Aqueous Mounting Medium with DAPI (Santa Cruz) prior to imaging. Videos were captured using A1R HD25 point scanning confocal with GaAsP and PMT detectors, equipped with an Apo TIRF 60x/1.49 NA objective lens and Ti2 Z-drive. 100 cells per transfected condition were manually scored into four morphological classifications (57): "Fragmented" refers to cells that contain spherical mitochondrial fragments with two or less short tubules present. "Short tubular" refers to cells containing a mixture of fragmented and short tubular mitochondria. "Long tubular" refers to cells with elongated mitochondria, but not fused into a mitochondrial mesh. "Interconnected" refers to cells with a highly interconnected network of mitochondrial filaments, with few isolated mitochondria.

Live cell confocal microscopy

Cells were stained with 1:1000 PKmito Deep Red (Spirochrome) at 37˚C for 30 min. Following three 1X PBS washes, cells were placed in Live Cell Imaging Solution (Invitrogen). Acquisition was performed using Nikon A1R HD25 confocal with GaAsP and PMT detectors and an Apo 60x/1.49 NA objective. Temperature, humidity, and CO_2 were controlled within an Oko-Lab chamber equipped with Live Cell™ and Solent Scientific controllers. Image acquisition done using NIS-Elements (Nikon Instruments Inc.) and analysis performed using Fiji (58). Time-lapse videos of mitochondria taken at 1 frame per 10 sec for 5 min.

Supporting Figures

Supporting Figure 1. SLC25A46 interacts with Opa1.

A. Strep-Opa1 co-elutes upon elution of bound SLC25A46-His. GDN extracts prepared from *P. pastoris* expressing SLC25A46-His, Strep-Opa1 or co-expressing SLC25A46-His and Strep-Opa1 were subjected to Ni-NTA column binding and elution.

B. The intralinks (black arcs) and monolinks (red circles) identified from crosslinking-mass spectrometry experiments are mapped on the domain diagrams of SLC25A46 and Opa1.

C. AlphaFold2 model for SLC25A46-Opa1 complex colored by pLDDT (red = high confidence, blue = low confidence).

Supporting Figure 2. Electrostatic and hydrophobic interactions are predicted to stabilize SLC25A46-Opa1 interaction.

A. Two different views of the SLC25A46-Opa1 interface predicted by AlphaFold 2 is enlarged on the right. Top: Predicted salt-bridge interactions between R257 of SLC25A46 and E561 of Opa1, and R347 of SLC25A46 and D565 of Opa1. Bottom: Adjacent to the salt bridges is a cluster of hydrophobic residues comprising of I229, I230, I349, Y357, V359, L360 of SLC25A46 and T576, F572, A569 of Opa1.

B. Intensity of the anti-His (SLC25A46) bands in the elution in Figure 2 were normalized against the corresponding bands from the input and plotted as a function of SLC25A46 concentration used in the reaction mixtures.

C. Presence of the nucleotides did not affect binding of SLC25A46 to Opa1. GDN extracts prepared from *P. pastoris* co-expressing SLC25A46-His and Strep-Opa1 were

incubated with 2 mM of the indicated guanosine nucleotide prior to StrepTactin binding and elution.

Supporting Figure 3. SLC25A46 interacts with Mfn2.

A. Domain diagrams of SLC25A46 and Mfn2 are depicted.

B. SLC25A46-His co-elutes upon elution of bound Mfn2-Strep. GDN extracts prepared from *P. pastoris* expressing Mfn2-Strep or co-expressing SLC25A46-His and Mfn2-Strep were subjected to StrepTactin column binding and elution.

C. Mfn2-Strep co-elutes upon elution of bound SLC25A46-His. GDN extracts prepared from *P. pastoris* expressing Mfn2-Strep or co-expressing SLC25A46-His and Mfn2-Strep were subjected to Ni-NTA column binding and elution.

D. Circular map of SLC25A46 and Mfn2 with the identified lysine-lysine crosslinks (black arcs). Crosslinker used is indicated. Crosslinks were identified between the cytosol-exposed N-terminal K60 of SLC25A46 and the HR1 lysines K416 and K420 of Mfn2.

E. The intralinks (black arcs) and monolinks (red circles) identified from crosslinking-mass spectrometry experiments are mapped on the domain diagram of Mfn2.

F. Model of the SLC25A46-Mfn2 interaction. The identified crosslinks are depicted as dotted lines in the AlphaFold 2 generated models of SLC25A46 and Mfn2. The N-terminal region of SLC25A46 comprising residues 1-83 is predicted to be disordered and is displayed as a hand-drawn cartoon. The transmembrane helices of Mfn2 were poorly modeled and are shown as cylinders.

G. GDN extracts prepared from *P. pastoris* co-expressing Mfn2-Strep and either SLC25A46-His WT, (Δ2-83)SLC25A46-His or disease mutants were subjected to StrepTactin (middle) or Ni-NTA (bottom) column binding and elution. (Δ2-83)SLC25A46

still interacts with Mfn2 as seen by co-elution of both proteins. Disease mutations did not abrogate binding of SLC25A46 to Opa1 or Mfn2.

H. GDN extracts prepared from *P. pastoris* co-expressing SLC25A46-His and Mfn2-Strep were incubated with 2 mM of the indicated guanosine nucleotide prior to StrepTactin binding and elution. Presence of the nucleotides did not affect binding of SLC25A46 to Mfn2.

Supporting Video 1.

Live-cell confocal microscopy of PKmito Deep Red-stained mitochondria in indicated HCT116 cell lines. Movies were taken at 15 sec per frame for 5 min. Playback at 4 frames per sec (37.5x real-time). Scale bar = 10 µm.

Supporting Figure 1

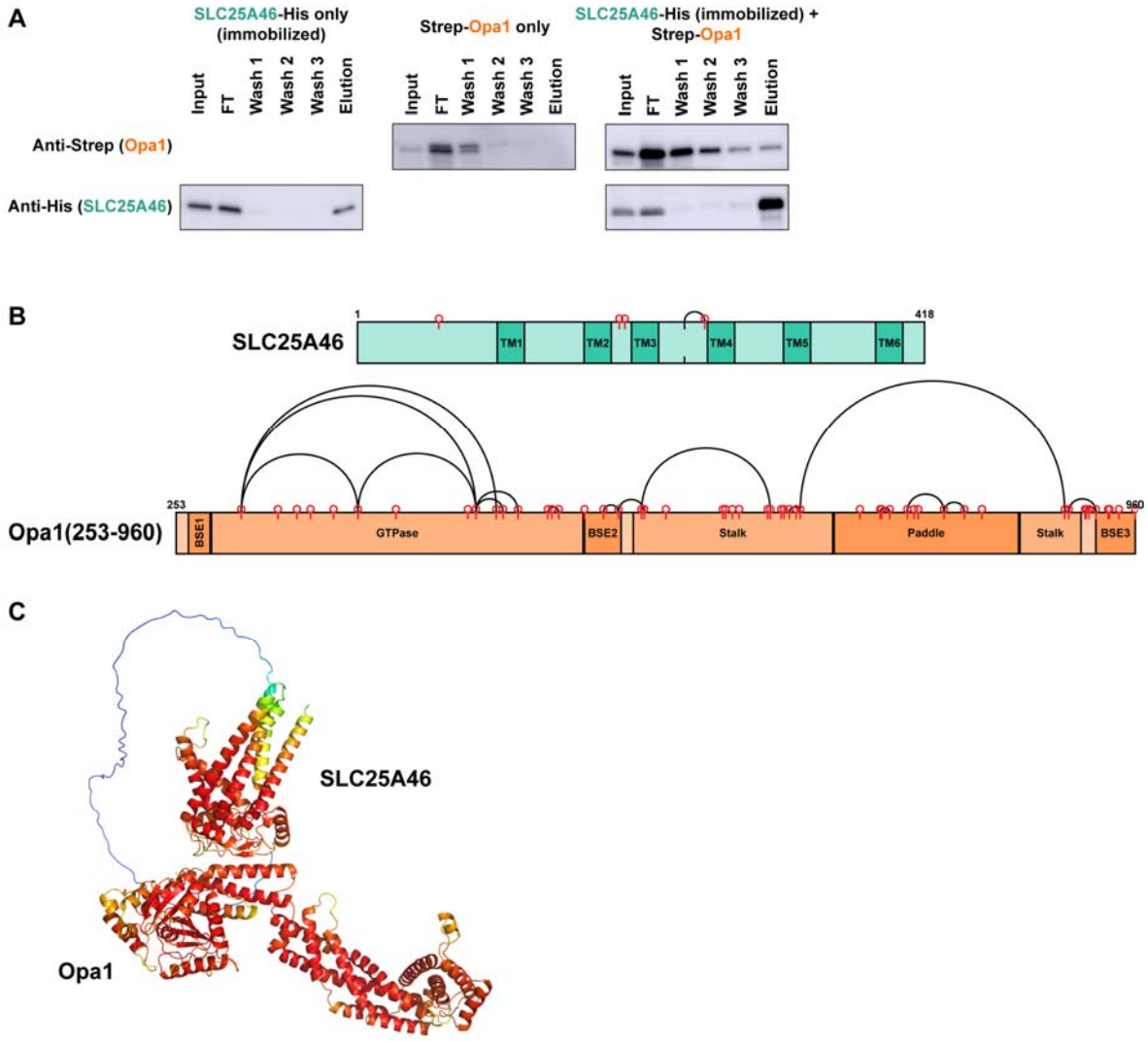

Supporting Figure 2

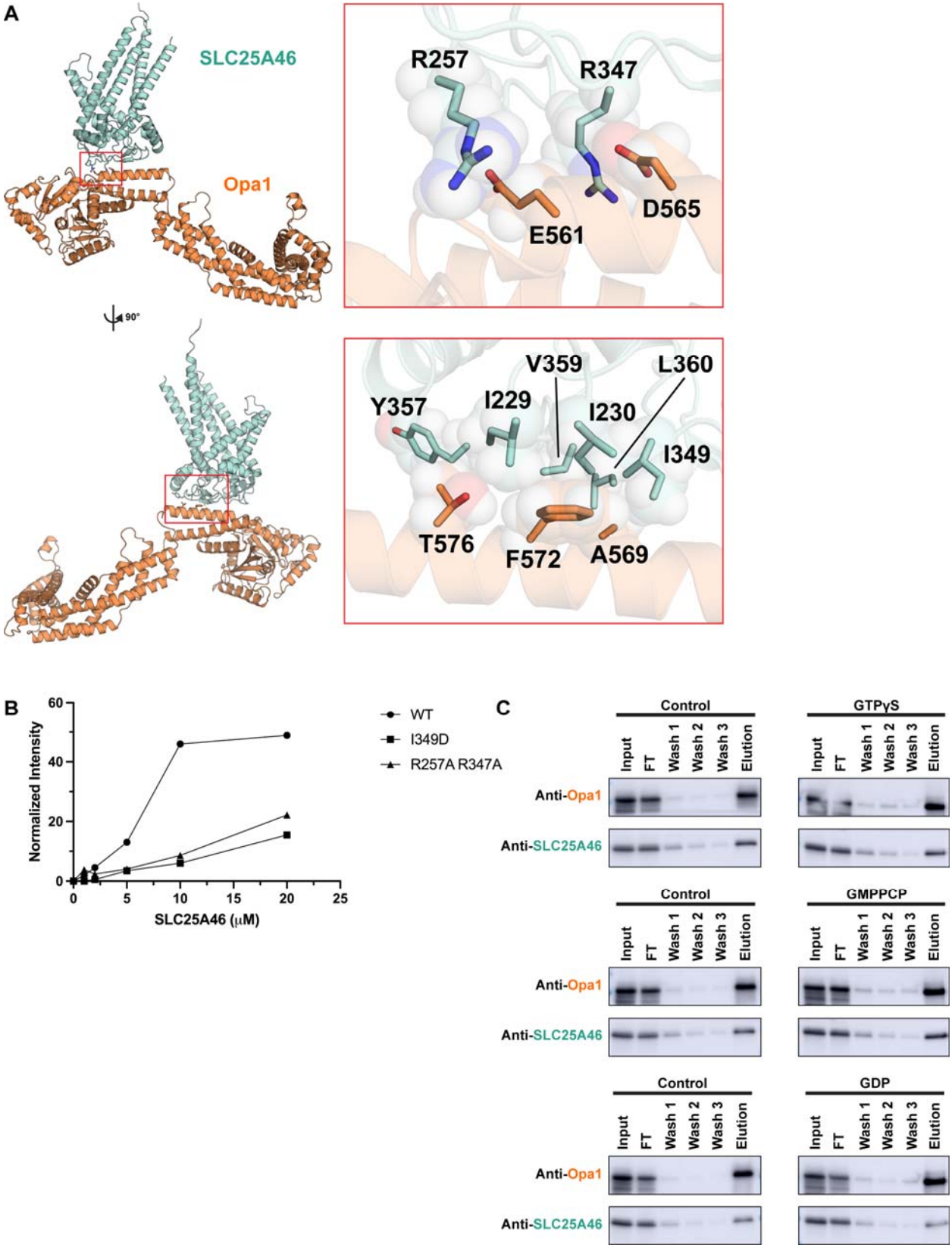
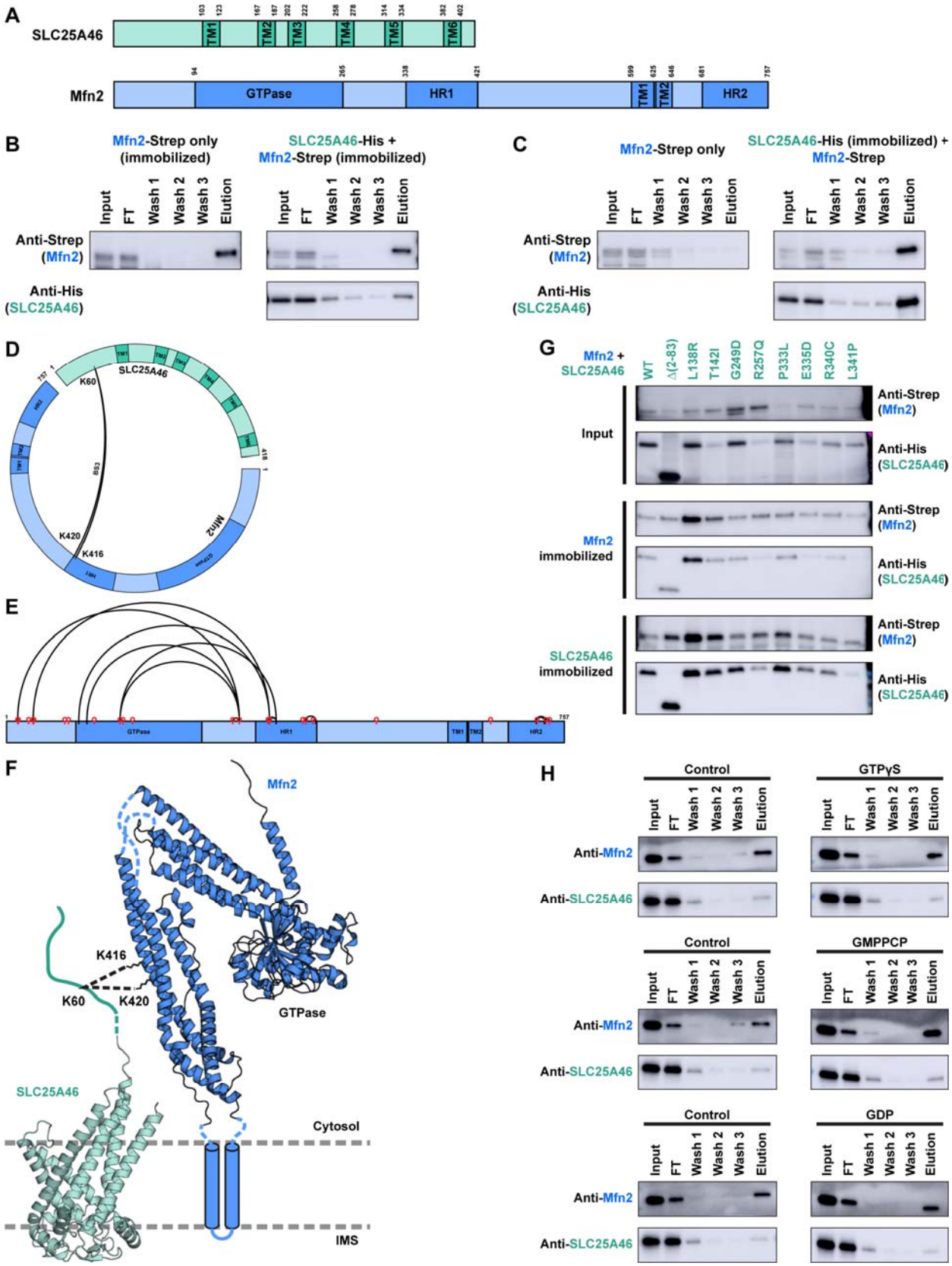
Supporting Figure 3